Self-amplified coherent spontaneous emission in the planar wiggler free-electron laser

B. W. J. McNeil and G. R. M. Robb
Department of Physics and Applied Physics, University of Strathclyde, Glasgow G4 0NG, Scotland
(Received 5 December 2001; revised manuscript received 15 January 2002; published 3 April 2002)

Coherent spontaneous emission (CSE) is a potentially important self-generated source of seed radiation in a free-electron laser (FEL) amplifier. A model is derived that describes CSE at the fundamental resonant frequency and its harmonics in a planar wiggler FEL. The subsequent self-amplification of the CSE is investigated in the nonlinear regime for a FEL amplifier configuration.

DOI: 10.1103/PhysRevE.65.046503 PACS number(s): 41.60.Cr

I. INTRODUCTION

In a single pass free-electron laser (FEL) amplifier the radiation to be amplified may be classified into three distinct types: radiation from an external coherent source such as a laser; the spontaneous emission arising from the shot noise in the electron pulse; and coherent spontaneous emission (CSE) arising from current gradients in the electron pulse. The latter two types are currently the only sources of radiation available for FEL amplification in regions of the spectrum where there are no external laser sources of sufficient power and/or coherence, e.g., in the vacuum ultraviolet and x ray.

FEL amplification of spontaneous radiation has been termed self-amplified spontaneous emission (SASE) [1,2] and amplification of coherent spontaneous radiation self-amplified coherent spontaneous emission (SACSE) [3,4]. When electron pulse current gradients are sufficiently large it has been predicted that SACSE can easily dominate the SASE interaction in an FEL amplifier. This dominance has already been demonstrated experimentally in the Cherenkov maser [5], a device with significant similarities to the FEL. Because the initial radiation source in the FEL SASE regime arises from noise, the radiation pulse structure following amplification may also exhibit a large degree of noise. Consequently, pulse to pulse reproducibility also suffers. In the SACSE regime, however, the initial radiation source is determined by the temporal current profile of the electron pulse. The amplified radiation in SACSE will therefore be intrinsically less noisy and exhibit greater pulse to pulse stability [4]. Thus, the SACSE regime of operation may be beneficial to users of short wavelength FELs, where radiation pulse noise and pulse to pulse stability may be an issue of experimental importance.

This paper presents what the authors believe is the first one-dimensional analysis of SACSE in a planar wiggler FEL amplifier. The analysis extends previous studies of SACSE that were carried out for helical wiggler configurations only [3,6,4]. Given the importance of including the effects of CSE in helical wiggler FEL configurations, it would seem timely to investigate the role of CSE in the planar wiggler FEL configuration, particularly as this is the preferred type of wiggler for most of the Compton regime FEL experiments and user facilities.

In a helical wiggler configuration there is no resonant radiation emission at harmonics of the resonant fundamental radiation frequency along the coaxial radiation-electron propagation direction of the wiggler axis [7]. On-axis interaction at harmonics may therefore be neglected in the helical wiggler. In contrast, in a planar wiggler configuration, significant on-axis radiation emission at harmonics of the fundamental may occur and the radiation-electron interaction at these harmonics may not be neglected [7].

Previous work has calculated the CSE from an electron pulse traversing a planar wiggler directly from the Liénard-Wiechert potentials [8] . Whereas, this work provides information of the CSE both on and off axis, it does not describe the radiation-electron interaction in the self-consistent way required to describe the stimulated emission due to the FEL mechanism.

The evolution of the self-consistent interaction between the electron pulse and the radiation field is described in this paper via the coupled Maxwell-Lorentz equations. The electrons interact with the radiation and static wiggler fields, their position and momentum evolution being described by the Lorentz force equation. The electron motion in the wiggler constitutes a current that acts as a source of the electromagnetic field, the evolution of which is described by Maxwell's wave equation. The on-axis harmonic radiation in the planar wiggler is due to an oscillatory axial ''jitter'' motion of the electrons about their mean velocity as they propagate along the wiggler axis [7].

To date, most analytical studies of the FEL have involved the averaging of the Maxwell-Lorentz equations over an interval equal to or greater than one wiggler period [7,9]. This averaging restricts the resolution of solutions to the system's evolution to time and spatial scales that are greater than the fundamental radiation period. As SACSE is a process that can only be described with reference to scales less than this period, the above averaging of the Maxwell-Lorentz equations destroys any information of SACSE in their solution.

In the work presented here, no averaging of the Maxwell-Lorentz equations is performed, allowing for a more accurate description of the FEL's evolution by including the effects of SACSE. Because the Maxwell-Lorentz equations are not averaged, the transverse electron dynamics are described in differential form. Furthermore, the radiation is described directly via its oscillatory field and not by the field envelope as in the averaged model. The more complex system of equations in this unaveraged model is the price to be paid for obtaining the extra information of sub-radiation period SACSE evolution.

The following work begins with the coupled Maxwell-

Lorentz equations from which the working system of equations used to model SACSE in the planar wiggler FEL are derived in detail. These working equations are scaled using the same scaling as previous averaged models [7] to allow for easy comparison. The equations are then solved in the absence of any radiation interaction upon the electron dynamics. This allows an expression to be derived for the CSE from an arbitrary electron pulse current profile. This expression is then used to investigate and compare the scaling of CSE and spontaneous radiation intensity as a function of frequency. The working equations are then solved numerically to investigate the radiation/electron interaction into the nonlinear SACSE regime for two different electron pulse current profiles.

II. THE MODEL

In what follows we consider the interaction between a pulse of electrons of mean energy $\gamma_r mc^2$, resonant with a plane, linearly polarized radiation field in a planar wiggler FEL configuration. The electric field, the wiggler magnetic field, and the transverse current density are given, respectively, as

$$\mathbf{E}(z,t)=\hat{\boldsymbol{x}}E_x(z,t)=\frac{1}{2}\hat{\boldsymbol{x}}\sum_{f=1}^{\infty}[\mathcal{E}_f(z,t)e^{if(k_1z-\omega_1t)}+\text{c.c.}], \tag{1}$$

$$\mathbf{B}_w(z)=-\hat{\boldsymbol{y}}B_w\sin k_wz, \tag{2}$$

$$\mathbf{J}_\perp=-ec\sum_{j=1}^{N}\boldsymbol{\beta}_\perp\delta(\boldsymbol{r}-\boldsymbol{r}_j(t)), \tag{3}$$

where N is the total number of electrons in the pulse with positions $\boldsymbol{r}_j(t)$ and transverse velocity $\boldsymbol{\beta}_\perp$, B_w is the wiggler magnetic field strength of period $\lambda_w=2\pi/k_w$ and the radiation electric field has been expanded as a sum of complex harmonic field envelopes of the fundamental resonant wave vector $k_1=2\pi/\lambda_1$, where

$$\lambda_1=\frac{\lambda_w}{2\gamma_r^2}(1+\overline{a_w^2}),$$

$\omega_1=ck_1$, and $\overline{a_w}=eB_w/\sqrt{2}mck_w$ is the rms wiggler deflection parameter.

A. Radiation evolution

For such a plane wave interaction the field evolution is described by the wave equation,

$$\left(\frac{\partial^2}{\partial z^2}-\frac{1}{c^2}\frac{\partial^2}{\partial t^2}\right)\boldsymbol{E}=\mu_0\frac{\partial\boldsymbol{J}_\perp}{\partial t}. \tag{4}$$

Substituting for the harmonic sum form of the electric field (1), assuming the electron and radiation pulses have equal cross-sectional areas, σ, and taking the scalar product with $\hat{\boldsymbol{x}}$, the wave equation (4) may be written:

$$\left(\frac{\partial^2}{\partial z^2}-\frac{1}{c^2}\frac{\partial^2}{\partial t^2}\right)\sum_{f=1}^{\infty}[\mathcal{E}_f(z,t)e^{if(k,z-\omega,t)}+\text{c.c.}]=\frac{2}{\epsilon_0c^2\sigma}\frac{\partial J_x}{\partial t}. \tag{5}$$

where

$$J_x=-ec\sum_{j=1}^{N}\beta_x\delta(z-z_j(t)). \tag{6}$$

The wave equation (5) may be rewritten in a more convenient form by changing to the scaled independent variables [9]:

$$\overline{z}=2k_w\rho z,\quad \overline{z_1}=\frac{2k_w\rho}{1-\overline{\beta_z}}(z-c\overline{\beta_z}t). \tag{7}$$

Here $c\overline{\beta_z}=\langle v_{z_0}\rangle$ is the initial mean z component of the electron velocity within the interaction region and ρ is the fundamental FEL parameter [1], defined as

$$\rho=\frac{1}{\gamma_r}\left(\frac{\overline{a_w}\omega_p}{4ck_w}\right)^{2/3}, \tag{8}$$

where $\omega_p=(e^2n_p/\epsilon_0m)^{1/2}$ is the plasma frequency for the peak electron number density of the electron pulse, n_p. The left-hand side of wave equation (5) then transforms, using the independent variables (7), to

$$8\rho^2k_w^2\frac{\overline{\beta_z}}{1-\overline{\beta_z}}\left(\frac{\partial}{\partial\overline{z}}+\frac{\partial}{\partial\overline{z_1}}\right)\left[\frac{\partial}{\partial\overline{z_1}}+\frac{1-\overline{\beta_z}}{2\overline{\beta_z}}\times\left(\frac{\partial}{\partial\overline{z}}+\frac{\partial}{\partial\overline{z_1}}\right)\right]\sum_{f=1}^{\infty}[\mathcal{E}_f(\overline{z,z_1})e^{(if/2\rho)(\overline{z}_1-\overline{z})}+\text{c.c.}]. \tag{9}$$

It is easily shown from Eq. (9) that when

$$\frac{1-\overline{\beta_z}}{2\overline{\beta_z}}\left|\frac{\partial\mathcal{E}_f(\overline{z,z_1})}{\partial\overline{z}}+\frac{\partial\mathcal{E}_f(\overline{z,z_1})}{\partial\overline{z_1}}\right|\ll\left|\frac{if}{2\rho}\mathcal{E}_f(\overline{z,z_1})+\frac{\partial\mathcal{E}_f(\overline{z,z_1})}{\partial\overline{z_1}}\right|, \tag{10}$$

or equivalently

$$\left|\frac{\partial\mathcal{E}_f(z,t)}{\partial z}+\frac{\partial\mathcal{E}_f(z,t)}{c\,\partial t}\right|\ll\left|\frac{\partial E_{xf}(z,t)}{c\,\partial t}\right|, \tag{11}$$

the partial differential term

$$\frac{1-\overline{\beta_z}}{2\overline{\beta_z}}\left(\frac{\partial}{\partial\overline{z}}+\frac{\partial}{\partial\overline{z_1}}\right)$$

may be neglected with respect to $\partial/\partial\overline{z_1}$ in the second bracketed differential term of Eq. (9). Inequality (11) is satisfied when the radiation envelope $\mathcal{E}_f(z,t)$ varies slowly as a function of $(z-ct)$ relative to the radiation field rate of change. Hence, $\mathcal{E}_f(z,t)\approx\mathcal{E}_f(z-ct)$ is a field envelope that does not change significantly in a radiation period, and consequently disallows any valid description of a radiation field counter-

propagating to the electron pulse. This analysis is similar to that of Ref. [10]. With this approximation the wave equation (5) may be written as:

$$\frac{\partial}{\partial \bar{z}_1}\left[\left(\frac{\partial}{\partial \bar{z}}+\frac{\partial}{\partial \bar{z}_1}\right)\sum_{f=1}^{\infty}\left[\mathcal{E}_f(\bar{z},\bar{z}_1)e^{(if/2\rho)(\bar{z}_1-\bar{z})}+\text{c.c.}\right]+\frac{1}{2\epsilon_0 c\sigma\rho k_w}J_x\right]=0. \tag{12}$$

The general solution for the bracketed term differentiated with respect to $\bar{z}_1$ in Eq. (12) is equal to a general function of $\bar{z}$ plus a constant. It can be seen from the zero source limit ($J_x\to 0$) that both the general function of $\bar{z}$ and the constant must be set equal to zero for energy and momentum conservation. Thus, the bracketed term differentiated with respect to $\bar{z}_1$ in Eq. (12) itself is equal to zero and we obtain

$$\left(\frac{\partial}{\partial \bar{z}}+\frac{\partial}{\partial \bar{z}_1}\right)E_x(\bar{z},\bar{z}_1)=\frac{e}{2\epsilon_0 mc\sigma}\frac{\bar{\beta}_z}{1-\bar{\beta}_z}\times\sum_{j=1}^{N}\frac{p_{xj}}{\gamma_j\beta_{zj}}\delta(\bar{z}_1-\bar{z}_{1j}(\bar{z})), \tag{13}$$

where we have reverted back to the simple radiation electric field via Eq. (1), introduced the x component of the electron momenta p_x in the definition of the current density (6) and transformed the Dirac delta function,

$$\delta(z-z_j(t))=2k_w\rho\frac{\bar{\beta}_z}{1-\bar{\beta}_z}\frac{\delta(\bar{z}_1-\bar{z}_{1j}(\bar{z}))}{\beta_{zj}}.$$

The magnetic component of the electromagnetic field may be obtained from the Maxwell equation,

$$\frac{\partial E_x}{\partial z}=-\frac{\partial B_y}{\partial t},$$

which, using the same approximation (11) as used in the wave equation above, may be written

$$B_y=\frac{E_x}{c}. \tag{14}$$

B. Electron evolution

The equation governing the electron motion in the combined wiggler magnetic and electromagnetic fields is the Lorentz force equation

$$\frac{d\boldsymbol{p}_j}{dt}=-e\left(\boldsymbol{E}+\frac{\boldsymbol{p}_j}{\gamma_j m}\times\boldsymbol{B}\right). \tag{15}$$

Substituting for the fields (1),(2),(14), and defining the variables:

$$\bar{p}_{xj}=\gamma_j\beta_{xj}, \tag{16}$$

$$\epsilon Q_j=\frac{1-\beta_{zj}}{\beta_{zj}}, \tag{17}$$

$$\epsilon=\frac{1-\bar{\beta}_z}{\bar{\beta}_z}, \tag{18}$$

$$A=\frac{eE_x}{\sqrt{2}mc\omega_p\sqrt{\gamma_r\rho}}, \tag{19}$$

$$\alpha=\left(\frac{2\rho\gamma_r}{\bar{a}_w}\right)^2, \tag{20}$$

the Lorentz equation (15) may be written in the convenient form

$$\frac{d\bar{p}_{xj}}{d\bar{z}}=-\frac{\bar{a}_w}{\sqrt{2}\rho}\left[\sin\left(\frac{\bar{z}}{2\rho}\right)+\epsilon Q_j\alpha A\right], \tag{21}$$

$$\frac{dQ_j}{d\bar{z}}=-\frac{\bar{a}_w}{\sqrt{2}\rho}\frac{\bar{p}_{xj}}{1+\bar{p}_{xj}^2}Q_j\left[2\sin\left(\frac{\bar{z}}{2\rho}\right)+\epsilon Q_j\left\{3\sin\left(\frac{\bar{z}}{2\rho}\right)-2\alpha A\right\}+\epsilon^2 Q_j^2\left\{\sin\left(\frac{\bar{z}}{2\rho}\right)-\alpha A\right\}\right]. \tag{22}$$

These equations are exact within the approximation (11) that allows the electromagnetic component of the magnetic field to be written as Eq. (14). The scaled arrival time of an electron at scaled position $\bar{z}$ is given by $\bar{z}_{1j}(\bar{z})$. The equation governing this variable is found from Eq. (7) to be

$$\frac{d\bar{z}_{1j}}{d\bar{z}}=1-Q_j=2\rho p_j, \tag{23}$$

where the last equality is introduced to allow comparison with previous models for CSE in a helical wiggler FEL [3]. When averaged over a fundamental radiation period, and in the relativistic limit $\epsilon\ll 1$, Eq. (22) gives rise to the usual ''pendulum equation'' description of the evolution of an electron in the combined wiggler/radiation field. At the fundamental frequency ($f=1$) the ponderomotive potential so formed has a period in $\bar{z}_1$ of $4\pi\rho$. Note also that the field variable A is of the same scaled form as in Ref. [3] when interpreted as an rms value.

In the absence of the radiation field, $A=0$, the equations are easily integrable and we obtain the usual solutions for an electron trajectory in a planar wiggler [7], which in terms of the variables used here are

$$\bar{p}_{xj}=\sqrt{2}\bar{a}_w\cos\left(\frac{\bar{z}}{2\rho}\right), \tag{24}$$

$$\epsilon Q_j = \left(1 - \frac{1 + 2\bar{a}_w^2 \cos^2(\bar{z}/2\rho)}{\gamma_j^2} \right)^{-1/2} - 1$$

$$\approx \frac{1 + 2\bar{a}_w^2 \cos^2(\bar{z}/2\rho)}{2\gamma_j^2}, \tag{25}$$

$$\bar{\beta}_z = \frac{2}{\pi} \frac{\sqrt{\gamma_r^2 - 1}}{\gamma_r} Ei\left(\frac{2\bar{a}_w^2}{\gamma_r^2 - 1} \right) \approx 1 - \frac{1 + \bar{a}_w^2}{2\gamma_r^2}, \tag{26}$$

where $Ei(x)$ is the complete elliptic integral of the second kind and the latter two approximations are in the relativistic limit $\gamma_{r,j} \gg 1$.

The equations (21)–(23) are amenable to a perturbation expansion in the parameter ϵ in the relativistic limit where $\epsilon \ll 1$. This has been carried out and results of numerical integration of the resultant first order equations in ϵ were compared with the results of a numerical integration for a planar wiggler model averaged over a wiggler period, again in the relativistic limit and for a constant amplitude radiation field. Both models are in excellent agreement. One immediate approximation that can be made by inspection in the relativistic limit $\epsilon \ll 1$, is the neglect of the last term of Eq. (22). For the purposes of this paper, little advantage is derived in reproducing the perturbation expansion and we use Eqs. (21)–(23) as our working equations for the electron interaction with the combined radiation/wiggler fields.

C. The scaled coupled model

Introducing the scaling of the previous section into the wave equation (13) we obtain

$$\left(\frac{\partial}{\partial \bar{z}} + \frac{\partial}{\partial \bar{z}_1} \right) A(\bar{z}, \bar{z}_1) = \frac{1}{\bar{n}_\parallel} \frac{\gamma_r}{\sqrt{2\bar{a}_w}} \sum_{j=1}^{N} \frac{\bar{p}_{xj}}{1 + \bar{p}_{xj}^2} \times \sqrt{\epsilon Q_j (\epsilon Q_j + 2)}\, \delta(\bar{z}_1 - \bar{z}_{1j}(\bar{z})). \tag{27}$$

Assuming the relativistic limit $\gamma_{r,j} \gg 1$ and substituting for solutions from (24)–(26) we obtain

$$\left(\frac{\partial}{\partial \bar{z}} + \frac{\partial}{\partial \bar{z}_1} \right) A(\bar{z}, \bar{z}_1) = \cos\left(\frac{\bar{z}}{2\rho} \right) \frac{1}{\bar{n}_\parallel} \sum_{j=1}^{N} \delta(\bar{z}_1 - \bar{z}_{1j}(\bar{z})). \tag{28}$$

This equation describes an electron-radiation coupling in which the radiation field is driven by the transverse motion of the electrons induced by the wiggler field only, and changes in energy of the electrons away from resonance do not affect the strength of the electron coupling to the radiation field.

Together, Eqs. (21)–(23) and Eq. (27) form the coupled set of differential equations describing the self-consistent electron-radiation evolution in a planar wiggler FEL. These equations are valid under the plane wave and the slowly varying envelope approximation of Eq. (11) or equivalently Eq. (14).

III. ANALYSIS

A. Coherent spontaneous emission

In the relativistic limit and in the absence of radiation fields the trajectory of an electron through the wiggler is found from Eq. (23) and Eqs. (25),(26) to be

$$\bar{z}_{1j}(\bar{z}) \approx \bar{z}_{1j0} - 2\rho\zeta \sin\left(\frac{\bar{z}}{\rho} \right), \tag{29}$$

where $\bar{z}_{1j0} = \bar{z}_{1j}(\bar{z} = 0)$, and

$$\zeta = \frac{\bar{a}_w^2}{2(1 + \bar{a}_w^2)}. \tag{30}$$

Substitution for Eq. (29) into the wave equation (28) allows the equation of the field generated by the jth electron to be written as

$$\left(\frac{\partial}{\partial \bar{z}} + \frac{\partial}{\partial \bar{z}_1} \right) A_j(\bar{z}, \bar{z}_1) = \cos\left(\frac{\bar{z}}{2\rho} \right) \frac{1}{\bar{n}_\parallel} \delta\left(\bar{z}_1 - \left[\bar{z}_{1j0} - 2\rho\zeta \sin\left(\frac{\bar{z}}{\rho} \right) \right] \right). \tag{31}$$

Applying the Laplace transform

$$\tilde{A}_j(\bar{z}, s) = \mathcal{L}\{A_j(\bar{z}, \bar{z}_1)\} = \int_0^\infty A_j(\bar{z}, \bar{z}_1) e^{-s\bar{z}_1} d\bar{z}_1, \tag{32}$$

with boundary condition given by $A_j(\bar{z}, \bar{z}_1 = 0) = 0$, yields

$$\frac{d\tilde{A}_j}{d\bar{z}} + s\tilde{A}_j = \frac{1}{\bar{n}_\parallel} \cos\left(\frac{\bar{z}}{2\rho} \right) e^{-s[\bar{z}_{1j0} - 2\rho\zeta \sin(\bar{z}/\rho)]}. \tag{33}$$

This equation may be solved with the initial condition $\tilde{A}_j(\bar{z} = 0, s) = 0$, to obtain

$$\tilde{A}_j(\bar{z}, s) = \sum_{f > 0, \text{odd}}^{\infty} \tilde{A}_{jf}(\bar{z}, s), \tag{34}$$

where

$$\tilde{A}_{jf}(\bar{z}, s) = -\frac{i\rho}{\bar{n}_\parallel} [\tilde{g}_-(s)(e^{i(f\bar{z}/2\rho)} - e^{-s\bar{z}}) - \tilde{g}_+(s)(e^{-i(f\bar{z}/2\rho)} - e^{-s\bar{z}})] e^{-s\bar{z}_{1j0}}, \tag{35}$$

and

$$\tilde{g}_\pm(s) = (-1)^{(f-1)/2} \times \frac{[J_{(f-1)/2}(\mp i 2\rho\zeta s) - J_{(f+1)/2}(\mp i 2\rho\zeta s)]}{f \pm i 2\rho s}.$$

In deriving this result the following Bessel function identities were required:

$$e^{ia\sin x}=\sum_{k=-\infty}^{\infty}J_k(a)e^{ikx},\quad J_{-n}(a)=(-1)^nJ_n(a),$$

$$J_n(-a)=(-1)^nJ_n(a).$$

The expression (35) is the Laplace transform of the fth (odd) harmonic contribution to the field from the jth electron. The derivation of the final result is assisted by now calculating $\tilde{A}_f$—the Laplace transform of the fth (odd) harmonic contribution to the field for the sum of the entire distribution of N electrons in an electron pulse of scaled duration in $\bar{z}_1$ of $\bar{l}_e=2\rho\omega\Delta t_e$, where Δt_e is the temporal duration of the pulse. We begin by describing the N electrons by a continuous charge distribution. In the limit of a continuous charge distribution, $\bar{z}_{1j0}$ is replaced by the dummy variable $\bar{z}_1'$ and the sum over the N electrons may be replaced by the integral over the charge weight function $\chi(\bar{z}_1')=I(\bar{z}=0,\bar{z}_1')/I_{\rm pk}$, where $I(\bar{z}=0,\bar{z}_1')$ is the electron pulse current with maximum value $I_{\rm pk}$ on entering the wiggler. Hence, the sum of the discrete electron model becomes

$$\frac{1}{n_\parallel}\sum_{j=1}^{N}(\cdots)\to\int_0^\infty\chi(\bar{z}_1')(\cdots)d\bar{z}_1'$$

in the continuous charge distribution limit, the lower limit on the integral being zero as $\bar{z}_{1j0}\geqslant 0\ \forall j$.

In this way we obtain

$$\tilde{A}_f=i\rho[\tilde{g}_+(s)(e^{-i(f\bar{z}/2\rho)}-e^{-s\bar{z}})-\tilde{g}_-(s)(e^{i(f\bar{z}/2\rho)}-e^{-s\bar{z}})]\int_0^\infty\chi(\bar{z}_1')e^{-s\bar{z}_1'}d\bar{z}_1'. \tag{36}$$

Note that the integral term is simply $\mathcal{L}\{\chi(\bar{z}_1)\}$, the Laplace transform of the charge weight function $\chi(\bar{z}_1)$. The Laplace transform convolution theorem

$$\mathcal{L}^{-1}\{\tilde{f}(s)\tilde{g}(s)\}=\int_0^{\bar{z}_1}f(u)g(\bar{z}_1-u)du \tag{37}$$

may now be applied to Eq. (36) by associating the functions $\tilde{g}_\pm(s)$ with $\tilde{g}(s)$ in Eq. (37) and noting the simple poles of $\tilde{g}_\pm(s)$ for inversion. Using the Laplace shifting theorem

$$\mathcal{L}^{-1}\{e^{-s\bar{z}}\mathcal{L}\{\chi(\bar{z}_1)\}\}=\chi(\bar{z}_1-\bar{z})H(\bar{z}_1-\bar{z}),$$

where $H(x)$ is the Heaviside function, allows the fth odd harmonic field component to be written as

$$A_f(\bar{\bar{z},z_1})=\rho\mathcal{J}_f\left[e^{-i[f(\bar{z}_1-\bar{z})/2\rho]}\int_{(\bar{z}_1-\bar{z})/2\rho}^{\bar{z}_1/2\rho}e^{if\theta}\chi(\theta)d\theta+\text{c.c.}\right], \tag{38}$$

where the transform $u\to 2\rho\theta$ has been made in Eq. (37) and

$$\mathcal{J}_f=(-1)^{(f-1)/2}[J_{(f-1)/2}(f\zeta)-J_{(f+1)/2}(f\zeta)].$$

Finally, the total scaled radiation field is obtained by summing over all odd harmonic contributions

$$A(\bar{\bar{z},z_1})=\sum_{f>0,\text{odd}}A_f(\bar{\bar{z},z_1}).$$

Note from Eq. (7) for the definitions of $\bar{z}$ and $\bar{z}_1$, that for a given electron pulse shape and width, the limits of the integral in Eq. (38) are ρ independent, so that $|A_f|^2\propto\rho^2$. Hence, from the scaling (8) and (19), the unscaled radiation intensity for the fth harmonic is proportional to the square of the electron beam density, i.e., the harmonic CSE is superradiant [9].

The field (38) is similar in form to that of CSE from a helical wiggler [3] for the fundamental frequency, $f=1$. The main difference being the Bessel function factor $\mathcal{J}_f$, familiar to planar wiggler FEL theory [7] and describing the reduced coupling of the radiation field to the electrons due to the latters' axial oscillatory motion as described by Eq. (29). The exponent of the exponential term outside the integral in unscaled variables is simply the harmonic field's phase $-if(k_1z-\omega_1t)$. It should be noted that the Bessel function factor $\mathcal{J}_f$ arises in previous theory as a consequence of averaging the equations over a wiggler period. However, no such averaging was performed here.

A radiation wave front propagates relative to the electron pulse with a scaled velocity $d\bar{z}_1/d\bar{z}=1$. Hence, at a scaled position $\bar{z}$ and time $\bar{z}_1$, only those regions of the electron pulse that lie within the interval in $\bar{z}_1$ between $\bar{z}_1$ and $\bar{z}_1-\bar{z}$ may contribute to the radiation field. This is the physical reason for the limits of the integral over the charge weight function $\chi(\theta)$ in Eq. (38). If these limits are incorporated as a difference of Heaviside functions within the integral, as in Ref. [3], then the integral may be written as a Fourier transform of the product of $\chi(\theta)$ with the difference of Heaviside functions. For $\bar{l}_e<\bar{z}_1<\bar{z}$, then the integral is simply the Fourier transform of the charge weight function $\chi(\theta)$.

For example, in this latter region, and for a rectangular charge weight function:

$$\chi(\bar{z}_1)=1\quad\text{for}\quad 0<\bar{z}_1<\bar{l}_e$$
$$=0\quad\text{otherwise}, \tag{39}$$

the harmonic field component

$$A_f(\bar{\bar{z},z_1})=\frac{2\rho}{f}\mathcal{J}_f\left[\sin\left(\frac{f(\bar{z}_1-\bar{z})}{2\rho}\right)-\sin\left(\frac{f(\bar{z}_1-\bar{z}-l_e)}{2\rho}\right)\right]. \tag{40}$$

The factor $1/f$ may be attributed to the electron pulse appearing effectively f times longer to the harmonic than to the fundamental frequency. Hence, the Fourier components of the pulse weighting function $\chi(\theta)$ driving the harmonic field are reduced. It is easily shown that this scaling also applies outside the interval $\bar{l}_e<\bar{z}_1<\bar{z}$. The total scaled field A is

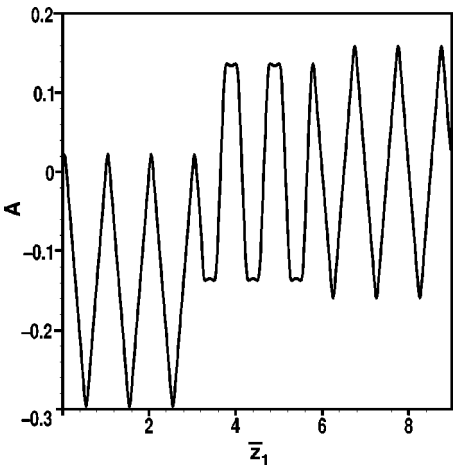

FIG. 1. The scaled field amplitude A plotted as a function of $\bar{z}_1$ for a rectangular charge weight function $\chi(\bar{z}_1)$ and for parameters $\bar{a}_w=1$, $\rho=0.0796$, $\bar{l}_e=3.2$, and $\bar{z}=5.8$.

plotted for a rectangular charge weight function of scaled duration $\bar{l}_e=3.2$ at scaled position $\bar{z}=5.8$ over the entire range $0<\bar{z}_1<\bar{l}_e+\bar{z}$ in Fig. 1.

Similarly, in the region $\bar{l}_e<\bar{z}_1<\bar{z}$, for a parabolic charge weight function defined by

$$\chi(\bar{z}_1)=-\frac{4}{\bar{l}_e^2}\bar{z}_1(\bar{z}_1-\bar{l}_e) \quad \text{for} \quad 0<\bar{z}_1<\bar{l}_e$$
$$=0 \quad \text{otherwise}, \tag{41}$$

the scaled harmonic field is given by

$$A_f(\bar{z},\bar{z}_1)=-\frac{16\rho^2}{f^2\bar{l}_e}\mathcal{J}_f\left[\cos\left(\frac{f(\bar{z}_1-\bar{z}-l_e)}{2\rho}\right)+\cos\left(\frac{f(\bar{z}_1-\bar{z})}{2\rho}\right)\right]. \tag{42}$$

In deriving Eq. (42) it has been assumed that the electron pulse length is sufficiently long, i.e., $\bar{l}_e \gg 4\pi\rho/f$. This relation holds for electron pulse lengths significantly longer than a radiation period.

A relative measure of harmonic intensity is obtained from the ratio $R_f=I_f/I_1$ where I_f is the intensity of the fth harmonic. For the rectangular charge weight distribution of Eq. (39) and for given values of ρ and $\bar{a}_w$ then from Eq. (40)

$$R_f^{\mathrm{CSE}}(\text{rectangular})=\frac{\mathcal{J}_f^2}{f^2\mathcal{J}_1^2}. \tag{43}$$

Similarly, from equation (42) for a parabolic charge weight distribution

$$R_f^{\mathrm{CSE}}(\text{parabolic})=\frac{\mathcal{J}_f^2}{f^4\mathcal{J}_1^2}. \tag{44}$$

An equivalent expression may be obtained for spontaneous emission due to shot noise, and which is valid for any pulse charge weight distribution,

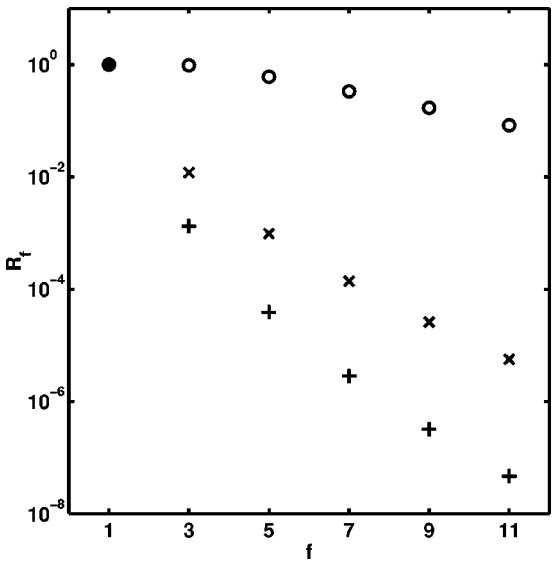

FIG. 2. The relative radiation intensities R_f plotted as a function of harmonic number f for $\bar{a}_w=1$. ○, Shot noise; ×, a rectangular charge weight function; and +, a parabolic charge weight function.

$$R_f^{\mathrm{SP}}=\frac{f^2\mathcal{J}_f^2}{\mathcal{J}_1^2}. \tag{45}$$

The latter expression has been derived from the expression for the on-axis spontaneous shot noise photon flux at the fth harmonic $\tilde{S}_f$ [11],

$$\frac{d^2\tilde{S}_f}{d\phi d\psi}=\frac{\sigma}{\hbar\omega_f}\frac{d^2I_f}{d\phi d\psi}=\alpha N_w^2\gamma_r^2\frac{\Delta\omega}{\omega}\frac{I}{e}F_f(\bar{a}_w), \tag{46}$$

where ϕ and ψ are the vertical and horizontal angles from the wiggler axis, α is the fine structure constant, N_w is the number of wiggler periods, $\Delta\omega/\omega=1/fN_w$ is the fractional linewidth, I is the electron beam current, and

$$F_f(\bar{a}_w)=\frac{2\bar{a}_w^2f^2}{(1+\bar{a}_w^2)^2}\mathcal{J}_f^2.$$

The relative intensities for both CSE, from a rectangular and a parabolic pulse, and spontaneous shot noise emission are plotted in Fig. 2 as a function of harmonic number f for a wiggler deflection parameter $\bar{a}_w=1$. It is seen that the relative intensity of CSE decreases significantly more rapidly than spontaneous shot noise with increasing harmonic number, and that CSE of the parabolic decreases more rapidly than the rectangular.

B. Self-amplified coherent spontaneous emission

The full set of coupled equations (21)–(23) and Eq. (27) are now solved self-consistently into the nonlinear regime and demonstrate that CSE may be amplified as it propagates through the electron pulse—self-amplified coherent spontaneous emission. Such an analysis has previously been carried out for a helical wiggler configuration [3] where only the

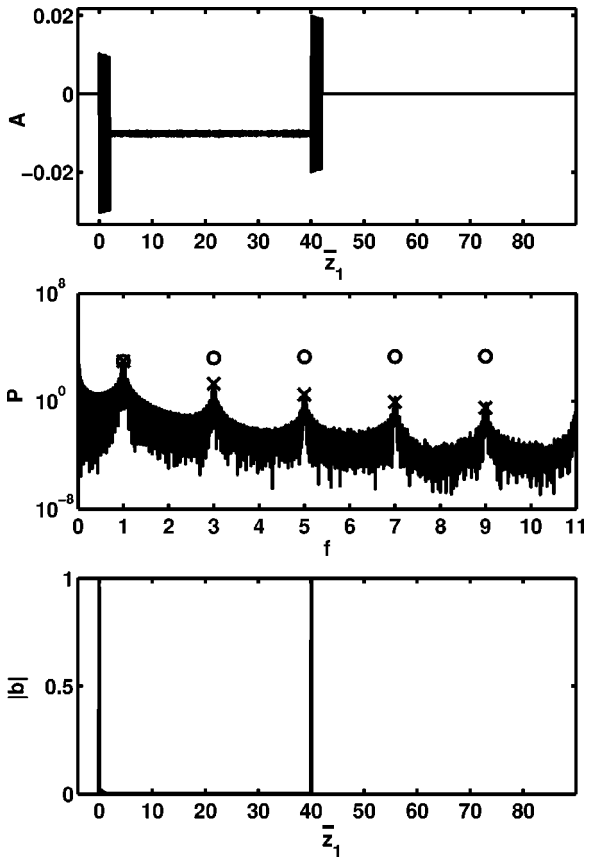

FIG. 3. The scaled field A as a function of $\bar{z}_1$; the scaled power spectrum P as a function of the scaled radiation frequency f; and the bunching parameter $|b|$ as a function of $\bar{z}_1$ for a rectangular charge weight distribution function $\chi(\bar{z}_1)$. The scaled distance through the wiggler is $\bar{z}=2$ and $\bar{a}_w=2$, $\gamma_r=100$, $\rho=10^{-2}$, $\bar{l}_e=40$ and the total electron pulse charge is $Q=2\ nC$. The relative radiation intensities R_f are plotted in the scaled power spectrum P as a function of harmonic number f for: ○, Shot noise; ×, CSE.

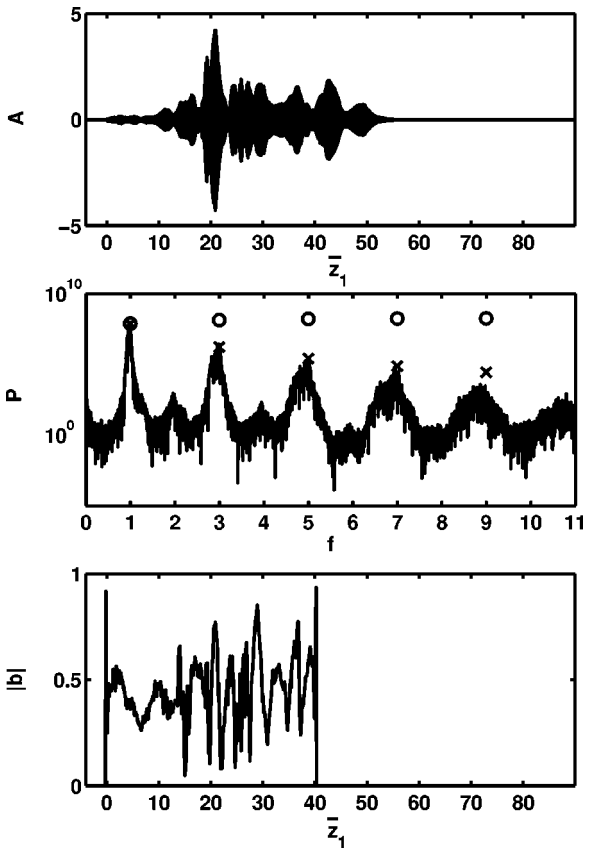

FIG. 4. The scaled field A as a function of $\bar{z}_1$; the scaled power spectrum P as a function of the scaled radiation frequency f; and the bunching parameter $|b|$ as a function of $\bar{z}_1$ for a rectangular charge weight distribution function $\chi(\bar{z}_1)$. The scaled distance through the wiggler is $\bar{z}=25$ and $\bar{a}_w=2$, $\gamma_r=100$, $\rho=10^{-2}$, $\bar{l}_e=40$ and the total electron pulse charge is $Q=2\ nC$. The relative radiation intensities R_f are plotted in the scaled power spectrum P as a function of harmonic number f for: ○, Shot noise; ×, CSE.

fundamental frequency of the radiation field is present and there is no axial jitter motion of the electrons. This allows the radiation field to be described by a complex pulse envelope. The streamline method of finite element analysis [12] was used to model the evolution of the radiation pulse in $\bar{z}_1$, with iteration forward in $\bar{z}$ being governed by a Crank-Nicolson scheme [13]. The radiation pulse was driven self-consistently by the electrons whose dynamical equations in the presence of the radiation pulse were solved by a Runge-Kutta routine.

The method used to solve the system of equations (21)–(23) and Eq. (27) describing the planar wiggler is essentially the same, except the solutions for a real (scaled) radiation field, not a complex envelope, and the transverse dynamics of the electrons must also be modeled via the equations for p_x.

Two sample solutions are now presented. The first is for a rectangular electron charge weight function, as described by Eq. (39) of the previous section, and the second is for a parabolic charge weight function given by Eq. (41).

In Figs. 3 and 4 the scaled radiation field amplitude A, the log of the scaled power spectrum P, and the modulus of the charge weighted bunching parameter $|b|$ are plotted at two scaled interaction distances $\bar{z}=2$ and $\bar{z}=25$ through a planar wiggler interaction region for a rectangular electron charge weight function $\chi(\bar{z}_1)$. The parameters used for this simulation were: $\bar{a}_w=2$, $\gamma_r=100$, $\rho=10^{-2}$, $\bar{l}_e=40$, total electron pulse charge of $Q=2\ nC$, and initial field amplitude $A(\bar{z}=0,\bar{z}_1)=0$. Shot noise, associated with the random electron distribution, was included in the model via the method described in Ref. [14] so that both noise and CSE sources were available for amplification. The bunching parameter b is similar to the bunching parameter as defined in previous averaged models [7] and is defined as

$$b(\bar{z},\bar{z}_1)=\frac{\sum_{\bar{z}_{1j}\in\Gamma}\chi_j e^{i\bar{z}_{1j}/2\rho}}{\sum_{\bar{z}_{1j}\in\Gamma}\chi_j}$$

where Γ defines an interval in $\bar{z}_1$ of one ponderomotive period at the fundamental frequency: $\bar{z}_1-2\pi\rho<\bar{z}_1<\bar{z}_1+2\pi\rho$

and $\chi_j=\chi(\bar{z}_{1j0})$. The parameter $f=\omega/\omega_1$ is the radiation frequency scaled with respect to the fundamental. For electrons distributed at the same position within Γ, $\bar{z}_{1j}$ = constant $\forall j$ and $|b|=1$. Conversely, for a uniform distribution of electrons within the interval Γ, $|b|=0$. Hence $|b|$ is bounded by the interval $0<|b|<1$.

In Fig. 3, at $\bar{z}=2$, it is seen that there has been little evolution of the field, *A*, except for the emission of CSE. (Note that, unlike Fig. 1, the periodic oscillations of the field are unable to be resolved in this plot, the period being approximately that of a ponderomotive potential $4\pi\rho\approx 0.13$. The solid shaded areas of the plot therefore delineate the envelope containing the field oscillations.) In the plot of the bunching parameter it is seen that $|b|\rightarrow 1$ as the interval Γ passes through the electron pulse edges at $\bar{z}_1=0$ and $\bar{z}_1=40$. This occurs when the interval Γ spans the electron pulse edge, only a fraction of the interval Γ is populated by electrons. This nonuniform distribution in Γ results in a bunching $|b|>0$, which, together with the large charge weight associated with a rectangular pulse (39), gives a large current gradient that is the source of the CSE. The scaled distance of $\bar{z}=2$ through the wiggler is relatively short with respect to the FEL instability and little radiation amplification or electron bunching induced by the FEL interaction has occurred. Hence, the CSE has not yet been amplified and the numerically calculated field is in very good agreement with the analytical analysis of the previous section. Note that there is a small contribution from the shot noise, which is apparent from a small noise signal in the field between $2<\bar{z}_1<40$. The dominance of the CSE contribution over that of shot noise is confirmed from the scaled power spectrum, where the harmonic intensity ratios, $R_f=I_f/I_1$, for both CSE and spontaneous scaling as given by equations (43) and (45) are also plotted. Here I_1 is that measured from the peak value of the scaled power spectrum at $f=1$. The peak values in the scaled power spectrum at the odd harmonics clearly concur with the CSE scaling. It can be seen from the plot for the field, *A*, that temporal structures exist on a scale significantly longer than that of the fundamental radiation period. This is also apparent from the plot of the scaled power spectrum where there exist significant contributions to the spectrum for $f<1$. This coherent emission at frequencies lower than the fundamental, $f=1$ is to be expected: in the limit where the radiation period is significantly greater than the electron pulse duration, the electron pulse appears pointlike and all electrons emit coherently at that frequency [8].

Figure 4 plots the same parameters as above for a greater distance through the wiggler, $\bar{z}=25$. The initial fields generated via shot noise and CSE have now grown significantly as has the electron bunching $|b|$ throughout the body of the electron pulse. The dominant feature of the radiation field is the presence of a large spike for $\bar{z}_1\approx 22$. This feature has also been predicted in helical wiggler FELs [3,4] and has been experimentally observed in a Cherenkov maser source [5], which has many similarities theoretically to the FEL. The origin of the spike, which is superradiant in nature [9], is in CSE emitted from the rear of the electron pulse, around $\bar{z}_1=0$, where the current gradient is large (see above). This radiation then propagates through the electrons being amplified and narrowing in width as it does so. Accordingly, this emission has been called SACSE [3]. A notable feature of the scaled power spectrum is the retention of the CSE scaling of the harmonic intensity ratios R_f well into the nonlinear regime.

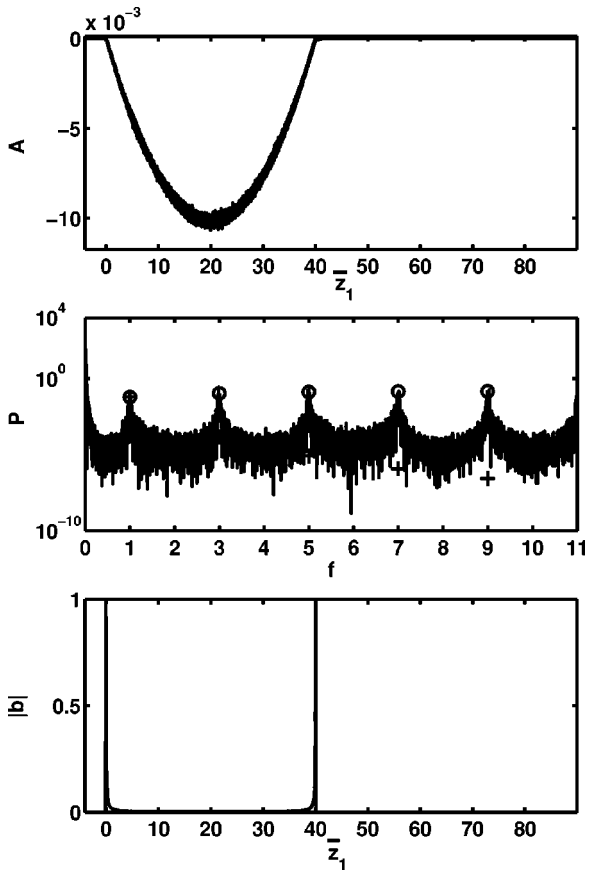

FIG. 5. The scaled field *A* as a function of $\bar{z}_1$; the scaled power spectrum *P* as a function of the scaled radiation frequency *f*; and the bunching parameter $|b|$ as a function of $\bar{z}_1$ for a parabolic charge weight distribution function $\chi(\bar{z}_1)$. The scaled distance through the wiggler is $\bar{z}=2$ and $\bar{a}_w=2$, $\gamma_r=100$, $\rho=10^{-2}$, $\bar{l}_e=40$ and the total electron pulse charge is $Q=2\ nC$. The relative radiation intensities R_f are plotted in the scaled power spectrum *P* as a function of harmonic number *f* for: ○, Shot noise; +, CSE.

The simulation for the parabolic charge weight function uses identical parameters to those of the rectangular above. The following plots the same information as the rectangular case. As with this case, it can be seen from Fig. 5 that at the beginning of the interaction, at $\bar{z}=2$, there are temporal structures present in the scaled field *A* with period significantly longer than the radiation period. This again manifests itself with significant power present in the scaled spectrum at frequencies below the fundamental ($f<1$). There is no notable presence of any CSE, however, and higher frequency emission appears mainly in the form of shot noise. It is easily shown from Eqs. (40) and (42) that the fundamental CSE intensity from the parabolic pulse is a factor $(8\rho/f\bar{l}_e)^2\approx 4$

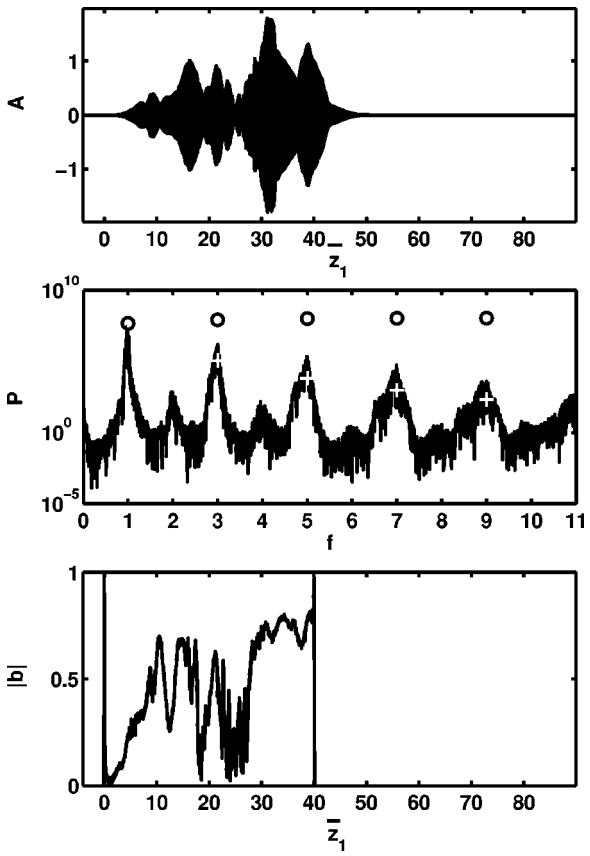

FIG. 6. The scaled field A as a function of $\bar{z}_1$; the scaled power spectrum P as a function of the scaled radiation frequency f; and the bunching parameter $|b|$ as a function of $\bar{z}_1$ for a parabolic charge weight distribution function $\chi(\bar{z}_1)$. The scaled distance through the wiggler is $\bar{z}=25$ and $\bar{a}_w=2$, $\gamma_r=100$, $\rho=10^{-2}$, $\bar{l}_e=40$ and the total electron pulse charge is $Q=2\ nC$. The relative radiation intensities R_f are plotted in the scaled power spectrum P as a function of harmonic number f for: ○, Shot noise; +, CSE.

$\times 10^{-6}$ smaller than from the rectangular pulse. The dominance of the shot noise over CSE is confirmed from the scaled power spectrum, with harmonic power ratios R_f conforming to the spontaneous shot-noise scaling (45). Although, as with the rectangular pulse, the bunching parameter $|b|$ is large at the pulse edges, the charge weighting function here is small. In changing from a rectangular to a parabolic charge distribution function, therefore, the current gradients that drive CSE have been reduced so that shot noise becomes the dominant emission process.

Plots of the same parameters into the nonlinear regime at $\bar{z}=25$ show from Fig. 6 that a spiking behavior in the radiation field is beginning to form in a way similar to the case of a rectangular charge weight function of Fig. 4. Perhaps the most significant point to note is the transition of the harmonic power ratios R_f from that of shot-noise scaling (45) to a scaling more like that of CSE (44). Analytic analysis of the equations governing the radiation/electron interaction into the nonlinear regime is not trivial and the scaling expected for R_f in this regime has not been derived. The nonlinear regime scaling clearly depends on other factors though, such as differing harmonic growth rates, at least in the linear regime [7]. The CSE-like scaling (44), resulting from the numerical analysis, however, suggests that the mechanisms that lead to CSE may also play an important role in the nonlinear regime of SACSE.

IV. CONCLUSIONS

Analytical and numerical studies of CSE and its amplification (SACSE) in a planar wiggler FEL in the one-dimensional (1D) plane wave limit have been presented. This is, to the authors' knowledge, the first such analysis for a planar wiggler FEL. The main difference between the planar and helical FEL amplifiers is the resonant on-axis harmonic radiation emission and amplification present in the planar wiggler and absent in the helical. In deriving the results, no averaging of either the wave equation or the equations governing the electrons' dynamics was performed as such averaging destroys CSE effects in the analysis. In the unaveraged equations the axial electron ''jitter'' motion associated with planar wigglers, and responsible for the on-axis harmonic emission, is allowed to evolve self-consistently with the radiation. This requires an extra differential equation, for the transverse momentum of each electron, above those of the averaged model.

Within the 1D plane wave assumptions, only one approximation was made in the derivation of the working equations. This may be written in the convenient form that relates the radiation magnetic field only to its electric field: $B_y=E_x/c$. This approximation is equivalent to the SVEA, i.e., that the radiation field envelope copropagating with the electron pulse may not change significantly in one radiation period.

The analysis of the wave equation in the presence of a noninteracting electron pulse gave a useful expression for the CSE field. It is worth remarking that from this analysis emerged the difference of Bessel functions factor, familiar to previous averaged planar wiggler models where it arises from the averaging process itself. It has been shown here, therefore, that the difference of Bessel functions factor is not a product of the averaging process but occurs at a more fundamental level. The analysis has shown that CSE powers decrease at a significantly higher rate with increasing harmonic number than those powers due to spontaneous shot-noise radiation. This is of no great surprise when one considers that it is the change in the pulse current over a wavelength that acts as a source of the CSE. The higher the harmonic, the smaller the change in current over its period and hence the smaller the source term driving the CSE at that harmonic.

It is remarkable that the same relative scaling of the harmonic powers persists well into the nonlinear regime. It would also appear that the CSE scaling occurs in the nonlinear regime independently of whether the greater source contribution is CSE or shot noise at the beginning of the interaction. This is perhaps indicative that the mechanisms that give rise to CSE retain their importance in the nonlinear regime and warrants further investigation.

Other attributes of planar wiggler SACSE have many similarities to those of a helical wiggler. Planar wiggler

SACSE is superradiant and pulses of CSE generated towards the rear of the electron pulse may propagate through it being amplified and forming a spike of radiation with intensity much greater than the saturation intensity predicted by the steady-state (cw) limit.

One of the great potential benefits of CSE is that it offers the possibility of a seed field with powers significantly greater than those due to shot noise. A further beneficial difference of CSE over shot noise is that the CSE radiation pulse structure may be predetermined by suitably preforming the electron pulse current. The SACSE will then form a well defined amplified pulse with a reproducibility determined by that of the electron pulse current as it enters the wiggler. This method offers a possible solution to the problem of pulse to pulse reproducibility in short wavelength FELs. The key to such a successful scheme is in preforming the electron pulse with sufficient current gradients so that CSE dominates shot noise. For example, it may be possible to make the electron pulse undergo a FEL interaction at an intermediate stage in their acceleration to high energy. This interaction would partially bunch the electrons at the intermediate energy resonant wavelength where there would be conventional laser sources to provide a well defined, intense seed field. (One would probably wish to limit this process by maximizing the ratio of bunching to energy spread, $|b|/\langle\gamma\rangle$, so induced. One can also envisage schemes that would bunch and then ''cool'' the electrons at this intermediate stage.) Further acceleration of the electron pulse will increase the resonant frequency of a final wiggler stage. In this wiggler the electron pulse current would have periodic modulations induced by the previous, lower energy FEL interaction. Although these modulations would be at a frequency below that of the resonant radiation, they may nevertheless act as a well defined source of CSE with an intensity above that of the shot noise.

ACKNOWLEDGMENTS

One of us, B.W.J.M., is very grateful to Lachlan McNeil for helpful discussions. The authors would like to thank the EPSRC for funding this work.

[1] R. Bonifacio, C. Pelligrini, and L. M. Narducci, Opt. Commun. **50**, 373 (1984).
[2] For review of current SASE experiments see: J. Feldhaus, J. Phys. IV **11**, PR2/237 (2001).
[3] B. W. J. McNeil, G. R. M. Robb, and D. A. Jaroszynski, Opt. Commun. **165**, 65 (1999).
[4] B. W. J. McNeil, G. R. M. Robb, and D. A. Jaroszynski, Nucl. Instrum. Methods Phys. Res. A **445**, 72 (2000).
[5] S. M. Wiggins, D. A. Jaroszynski, B. W. J. McNeil, G. R. M. Robb, P. Aitken, A. D. R. Phelps, A. W. Cross, K. Ronald, N. S. Ginzburg, V. G. Shpak, M. I. Yalandin, S. A. Shunailov, and M. R. Ulmaskulov, Phys. Rev. Lett. **84**, 2393 (2000).
[6] S. Krinsky, Phys. Rev. E **59**, 1171 (1999).
[7] See, for example, R. Bonifacio, F. Casagrande, G. Cerchioni, L. De Salvo Souza, P. Pierini, and N. Piovella, Riv. Nuovo Cimento **13**, 9 (1990), and references therein.
[8] C. P. Neuman, W. S. Graves, and P. G. O'Shea, Phys. Rev. ST Accel. Beams **3**, 030701 (2000).
[9] R. Bonifacio, B. W. J. McNeil, and P. Pierini, Phys. Rev. A **40**, 4467 (1989).
[10] R. Bonifacio, R. M. Caloi, and C. Maroli, Opt. Commun. **101**, 185 (1993).
[11] K. J. Kim, *X-ray Data Booklet*, http://xdb.lbl.gov/Section2/Sec_2-1.html
[12] C. Johnson, *Numerical Solution of Partial Differential Equations by the Finite Element Method* (Cambridge University Press, Cambridge, 1995).
[13] E. A. Huebner, E. A. Thornton, and T. G. Byrom, *The Finite Element Method for Engineers* (Wiley, New York, 1995).
[14] C. Penman and B. W. J. McNeil, Opt. Commun. **90**, 82 (1992).